Effects of Impact Deflection on Hazardous Asteroids: The Role of Asteroid Interior Structure

Yun Zhang*, **Yan Liu***, **Junfeng Li***, **Hexi Baoyin***

*Tsinghua University, Beijing, China,

The 4th IAA Planetary Defense Conference(April 13-17, 2015), Frascati, Roma, Italy

Abstract

The kinetic impact deflection would result in a number of unexpected hazardous fragments. For this reason, understanding the outcome of impacts is fundamental to assess the effects of this mitigation technique. Previous studies indicate that the internal structure of asteroid has significant influence on impact process and subsequent collisional evolution. The rubble-pile targets respond to an impact attempt quite differently than monolithic targets. In this paper, we explore numerically the aftereffects of kinetic impact mitigation on both rubble-pile and monolithic asteroids of 1 km in size. The process of hyper-velocity impact of a small artificial projectile on an asteroid target is investigated with the material point method (MPM). As a particle-in-cell method, MPM can efficiently solve the problems involving in extremely large deformation owing to its prominent advantages of dealing with fracture, fragmentation and moving material interface. In order to evaluate the impact threat of the resulting fragments pose to the Earth, the impact outcomes is transferred to an circumsolar orbit of hazardous asteroid. A parallel *N*-body code is applied to propagate the evolution of these fragments in the solar system until the predetermined date of impact. The hazard assessment is implemented by analyzing the minimum orbit intersection distance between the fragments and the Earth. As expected, the collision outcomes proved to be very dependent on the internal structure of asteroid. The fragments produced from the rubble-pile target is more disperse than the monolithic one. The hazard assessment implies that there are still a lot of small fragments pose threat to the Earth after the impact deflection, especially for the monolithic body.

Numerical technique

Fragmentation phase

Numerical code: MPM3D [1]

- An extension of particle-in-cell method: one set of Lagrangian points and one Eulerian background grid are used for discretization in MPM (as shown in Fig.1)
- Lagrangian points carry all the physical variables (i.e., mass, density, velocity, stress, strain)
- Eulerian background grid is used to solve momentum equations and to calculate spatial derivatives

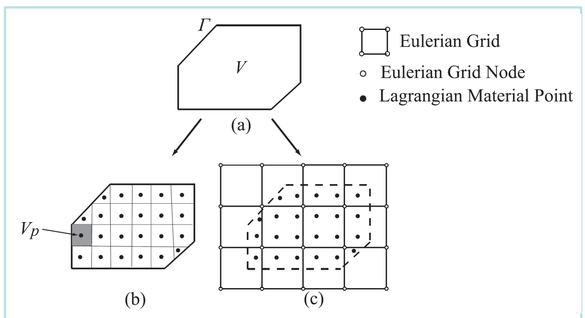

Fig.1 Schematic diagram of discretization in MPM

Gravitational phase

Numerical code: parallel *N*-body code

- Integration method: a leapfrog scheme
- Contact treatment: soft-sphere discrete element method[3]
- Hierarchical time steps and parameters:
  For dense particle package, $\Delta t \sim 1$ ms; for rapid collisionless particle, $\Delta t \sim 1$ s
  Each collision (or contact) is solved with its own parameters, which is calculated by the velocity and mass of the collisional pair with fixed coefficients of restitution.
- Merge algorithm: A group of particles are allowed to merge only if they reach the relative equilibrium state.
- Drawing force: between the particles in the same unfractured part; in the form of linear elasticity.

Hand off between two phases

- Merge in the Eulerian background grid (in order to reduce the computation time, merge is necessary):
  Using conservation law of mass and momentum, we merge all particles in one Eulerian background grid to a single spherical particle when their relative speed is smaller than their mutual escape speed.
- Merge in the unfractured part:
  For monolithic target, through continued expansion of the size of background grid, the particles in the grid is merged when all the particles belong to the same unfractured fragment. The procedure is repeated until no more merge can be done (as shown in the first row of Fig.2b and c).
  For rubble-pile target, a rubble is allowed to merge as a single sphere with the initial radius when the fraction of the damaged mass is smaller than 5% (as shown in the second row of Fig.2b and c).

Simulation setup

Material parameters

- Target: (500 m in diameter, ρ = 2.44 g/cm^3)
  Brittle rock : Holmquist-Johnson-Cook model[2]
  Numerical resolution: ~ 1,000,000 particles
- Projectile: (10 m in diameter , ρ = 2.77 g/cm^3)
  Aluminum[3]: Johnson-Cook strength model, Mie-Grüneisen EOS
  Numerical resolution: ~ 100 particles
- Soft-sphere DEM
  Normal coefficient of restitution is 0.5, tangential coefficient of restitution is 1 (smooth)
- The number of particles in the beginning of gravitational phase
  Monolithic target: ~ 11000 particles ($M_{asteroid} = 1.5985 \times 10^{11}$ kg, merge diameter: ~5m)
  Rubble-pile target: ~ 15000 particles ($M_{asteroid} = 1.5996 \times 10^{11}$ kg, merge diameter: ~5m)
- Drawing force between the same unfractured fragment
  When the particles of the same unfractured (undamaged) fragment start to leave each other, the attraction force $F = k\Delta x$ begin to work, where Δx is the distance between the surface of neighboring particles, $k \sim 10000$ N/m

Rubble-pile structure

- Size distribution: power law (maximum radius is 50 m, minimum radius is 12 m)
- Formation: the rubbles initially are randomly distributed in space and collapse due to gravitational interaction
- Mass and density keep the same as the monolithic one (the radius of the rubble-pile asteroid become larger because of its high level of macroporosity (~ 40%) in this structure)

PHA orbit and collision setup

- Orbital parameters: a = 1.726 AU, e = 0.571, i = 1.218°, Ω = 253.964°, ω = 73.162°
- Lead time ~ 10 years, deflection requirements ~ 0.01 m/s
- Impact velocity: v_{imp} = 2 km/s (both head-on), in the opposite direction to the orbital velocity
- Solar gravitational system: the Sun, the eight planets, and the moon

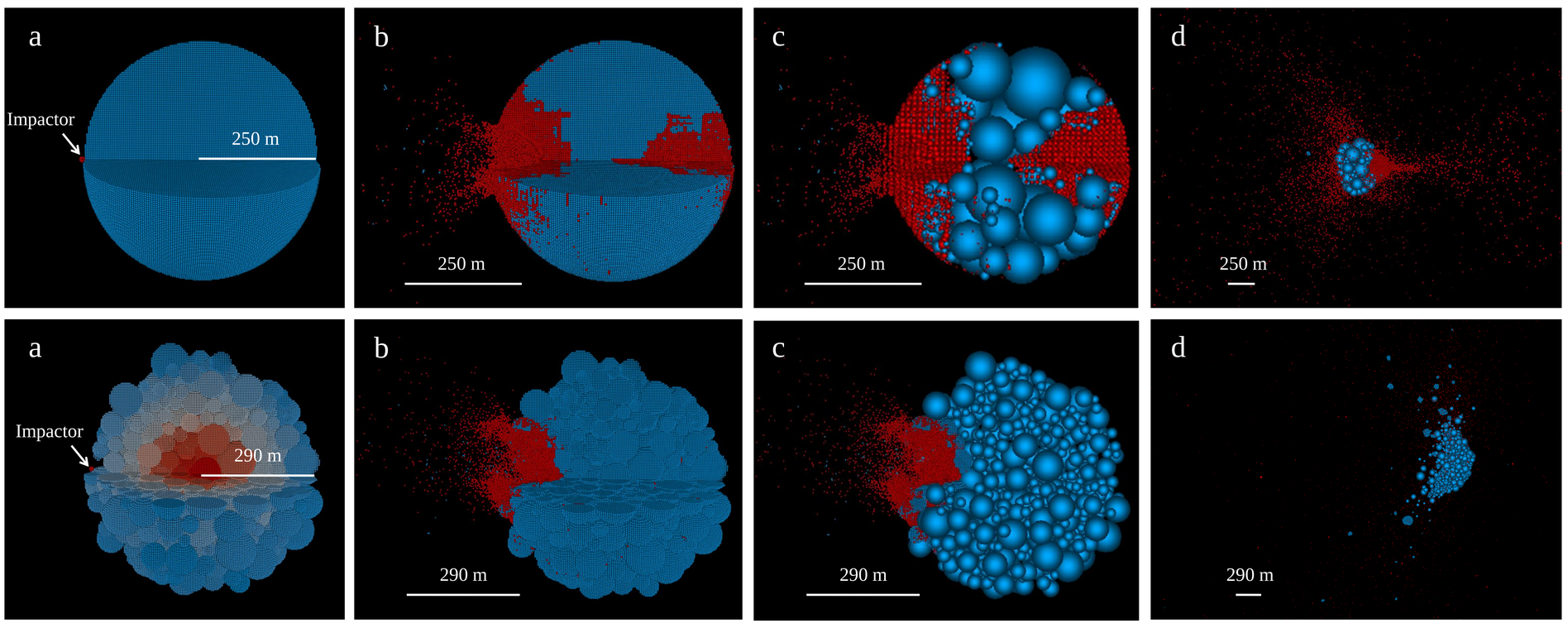

Fig.2 Snapshots of the fragmentation phase and the gravitational phase for two different internal structures (top: monolithic; bottom: rubble-pile). From left to right: (a) initial configuration of impact geometry (the color of rubble-pile model denotes the distance from its center); (b) last instant of the fragmentation phase seen 3 s after impact (blue is unfractured part, and red is fully damaged part); (c) first instant at the beginning of the gravitational phase which is converted from the output of fragmentation phase impact (the color coding is the same as in (b)); (d) the evolution of the resulting fragments 1000 s later (the color coding is the same as in (b)). In the first three frames, a quarter of the asteroid body is cut out.

Collision outcomes

The largest remnant

Table 1 Summary of the largest remnant's mass and ejection speed

Internal Structure	Specific impact energy Q (J/kg)	$M_{lr}/M_{asteroid}$	$[\Delta v_t \ \Delta v_n \ \Delta v_h]$ (m/s)
Monolithic target	21.822	0.905	[− 0.090 − 0.003 − 0.003]
Rubble-pile target	21.807	0.853	[− 0.127 − 0.003 − 0.012]

Size and ejection speed distributions of fragments

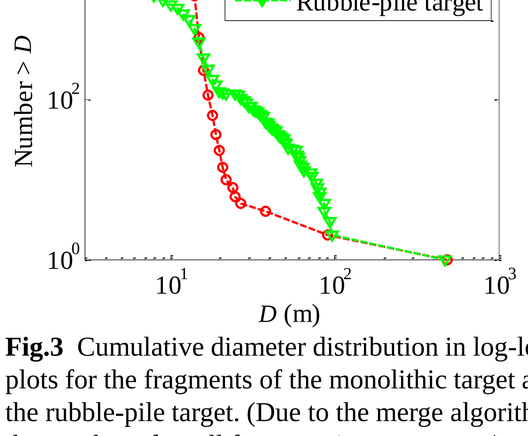

Fig.3 Cumulative diameter distribution in log-log plots for the fragments of the monolithic target and the rubble-pile target. (Due to the merge algorithm, the number of small fragment is not accurate)

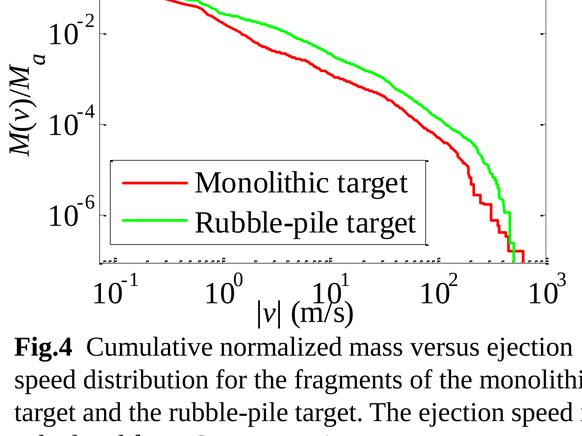

Fig.4 Cumulative normalized mass versus ejection speed distribution for the fragments of the monolithic target and the rubble-pile target. The ejection speed is calculated from Guass equations.

Orbital elements distributions of fragments

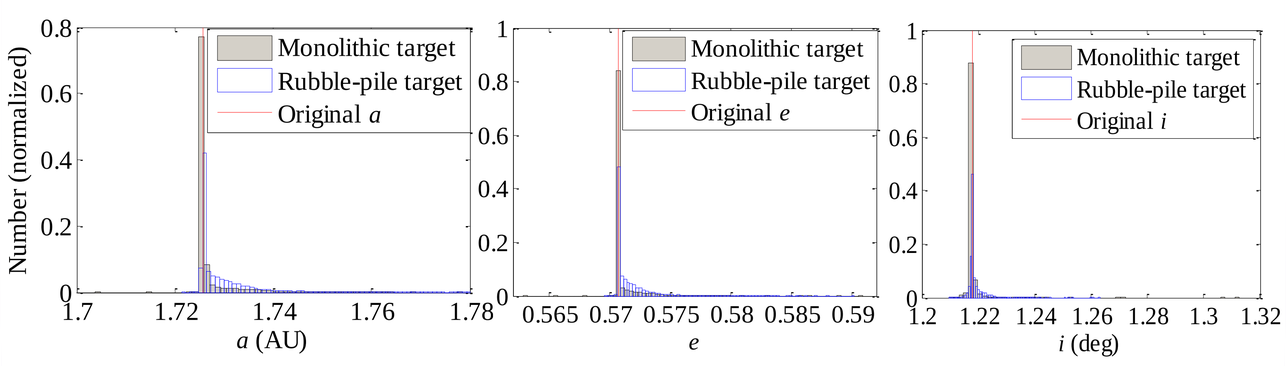

Fig.5 Histograms of the semimajor axis, eccentricity, and inclination of the fragments for the two target.

Hazard assessment

Differences in orbital elements of fragments

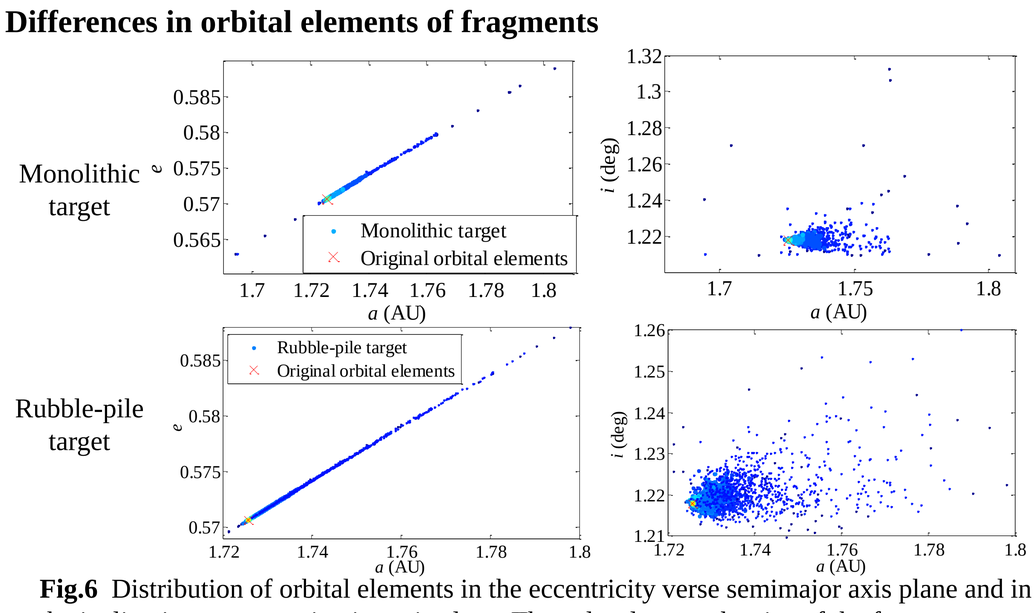

Fig.6 Distribution of orbital elements in the eccentricity verse semimajor axis plane and in the inclination verse semimajor axis plane. The color denotes the size of the fragments.

Expected damage

(Since the size of asteroid used in this study is about 100 m, the resulting fragments only cause airburst events. Thus, the airburst energy is used to evaluate the damage)

Table2 Estimate value of the damage (which is assessed using a web-based computer program[4])

Diameter (m)	Airburst energy (MT)	Number	
< 20 m	0 ~ 0.2	102: 4.95 m - 19.0 m(M)	22: 6.1 m - 16.5 m (R)
20m ~ 40 m	0.2 ~ 2.7	2: 20.2 m, 21.6 m (M)	2: 20.3 m, 39.0 m (R)

Total impact energy: ~ 6.49 MT for monolithic target, ~ 4.32 MT for rubble-pile target.

Conclusions

- Rubble-pile target leads to a smaller largest remnant, and the collisional process in this body is more efficient in transferring kinetic energy to the largest remnant.
- Compared with the rubble-pile target, the size distributions of fragments in the case of monolithic one lack of intermediate-sized bodies.
- The ejection speed and the orbital element distribution is more disperse for the rubble-pile body than for the monolithic body.
- The expected damage caused by the deflected monolithic target is larger than the rubble-pile target because of the exist of numerous small dangerous fragments.

References

[1] Liu P, Liu Y, Zhang X, et al. (2015) International Journal of Impact Engineering, 75: 241-254. [2] Holmquist TJ, Johnson GR, Cook WH. 14th International Symposium on Ballistics, Quebec, Candan, 26-29 September, 1993. [3] Schwartz SR, Richardson DC, Michel P. (2012) Granular Metter, 14: 363-380. [4] Collins GS, Melosh HJ, Marcus RZ. (2005) Meteoritics & Planetary Science, 40: 817-840.

Acknowledgements

This work was supported by the National Basic Research Program of China (973 Program, 2012CB720000) and the Tsinghua University Initiative Scientific Research Program (Grant No. 20131089268).